AGU PUBLICATIONS

Geophysical Research Letters

RESEARCH LETTER
10.1002/2014GL062162

Key Points:
- Strong roughness dichotomy between smooth and cratered plains is observed
- Scale-dependence of roughness contrasts suggests a thicker regolith versus the Moon
- Roughness signatures reveal different generations of smooth plain units

Correspondence to:
M. A. Kreslavsky,
mkreslav@ucsc.edu

Citation:
Kreslavsky, M. A., J. W. Head, G. A. Neumann, M. T. Zuber, and D. E. Smith (2014), Kilometer-scale topographic roughness of Mercury: Correlation with geologic features and units, *Geophys. Res. Lett.*, *41*, 8245–8251, doi:10.1002/2014GL062162.

Received 8 OCT 2014
Accepted 17 NOV 2014
Accepted article online 18 NOV 2014
Published online 8 DEC 2014

Kilometer-scale topographic roughness of Mercury: Correlation with geologic features and units

Mikhail A. Kreslavsky[1,2], James W. Head[3], Gregory A. Neumann[4], Maria T. Zuber[5], and David E. Smith[5]

[1]Earth and Planetary Sciences, University of California, Santa Cruz, California, USA, [2]Moscow State University of Geodesy and Cartography, Moscow, Russia, [3]Department of Geological, Environmental and Planetary Sciences, Brown University, Providence, Rhode Island, USA, [4]Solar System Exploration Division, NASA Goddard Space Flight Center, Greenbelt, Maryland, USA, [5]Department of Earth, Atmospheric and Planetary Sciences, MIT, Cambridge, Massachusetts, USA

Abstract We present maps of the topographic roughness of the northern circumpolar area of 30 Mercury at kilometer scales. The maps are derived from range profiles obtained by the 31 Mercury Laser Altimeter (MLA) instrument onboard the MErcury Surface, Space 32 ENvironment, Geochemistry, and Ranging (MESSENGER) mission. As measures of 33 roughness, we used the interquartile range of profile curvature at three baselines: 0.7 km, 34 2.8 km, and 11 km. The maps provide a synoptic overview of variations of typical 35 topographic textures. They show a dichotomy between the smooth northern plains and 36 rougher, more heavily cratered terrains. Analysis of the scale dependence of roughness 37 indicates that the regolith on Mercury is thicker than on the Moon by approximately a 38 factor of three. Roughness contrasts within northern volcanic plains of Mercury indicate a 39 younger unit inside Goethe basin and inside another unnamed stealth basin. These new 40 data permit interplanetary comparisons of topographic roughness.

1. Introduction

Synoptic maps of topographic roughness of planetary surfaces have proven to be a useful tool for geological studies of various planets. First, roughness maps provide a convenient large-scale overview of small-scale textures. Second, roughness maps help focus on typical topographic textures rather than on specific or unusual features. Topographic roughness depends on spatial scale, and this dependence also contains important information about geology, surface processes, and history. Multiscale roughness maps derived from laser altimeter data have revealed significant new facts about the geologic and climate history of Mars [*Kreslavsky and Head*, 2000, 2002] and geologic processes on the Moon [*Rosenburg et al*., 2011; *Kreslavsky and Head*, 2012; *Kreslavsky et al*., 2013]. Roughness maps fully utilize the high ranging precision and high along-orbit resolution of the data from orbital laser altimeters, while typical topographic maps derived from these data are characterized by lower absolute elevation accuracy due to imperfections in the knowledge of the orbit and gaps between orbital profiles.

A similar roughness mapping approach has been applied to data from Mercury Laser Altimeter (MLA) [*Cavanaugh et al*., 2007; *Zuber et al*., 2012] onboard orbital MErcury Surface, Space ENvironment, Geochemistry, and Ranging (MESSENGER) mission to Mercury by *Yang et al*. [2013], who produced the first roughness maps of the northern hemisphere of Mercury covered with MLA data and who described the roughness signatures of the major geologic features. In the present work, we apply a similar (but not the same) technique to the northern circumpolar zone (84°N–65°N) only, where the amount and quality of the data are the highest. We present these new roughness maps and discuss a few selected primary inferences about processes that shape and modify the surface.

2. Mapping Roughness

The roughness mapping technique that we use here is very similar to the technique that we have applied to the lunar laser ranging data [*Kreslavsky et al*., 2013]. Utilizing this approach facilitates comparison with the Moon. We start with the entire set of topographic profiles along MESSENGER orbits obtained by MLA from the orbit insertion in March 2011 through September 2013. This data set is the Scientific Data Record from the MLA archive in the Planetary Data System. It contains about ~8.8×10^6 good data points, less than 1/100 of the data volume used for the Moon. Due to the high eccentricity of the MESSENGER orbit and the periapsis at

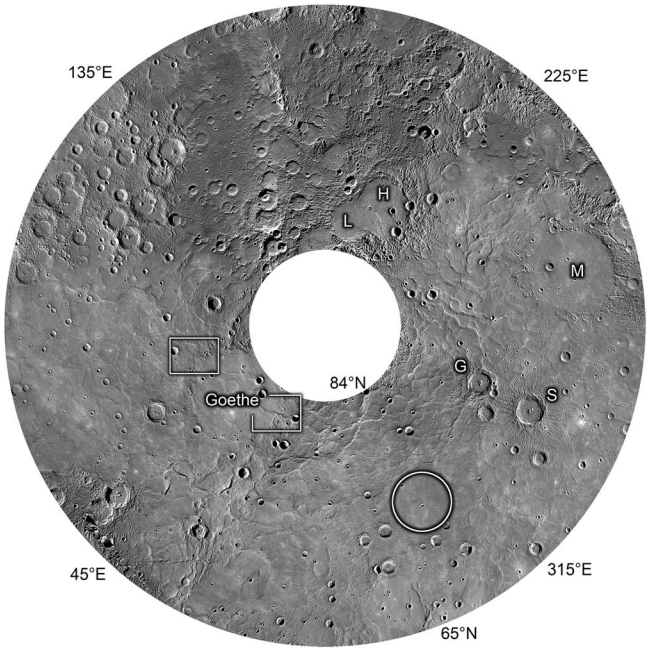

Figure 1. MDIS mosaic of the northern circumpolar region of Mercury from 84°N to 65°N in polar Lambert azimuthal equal area projection. Letters mark the following craters or basins: H, Henri (D = 160 km); L, Lismer (D = 140 km); M, Mendelssohn (D = 290 km); G, Gaudi (D = 80 km); and S, Stieglitz (D = 100 km). The circle marks a smooth ghost crater (D = 200 km) discussed in the text. Boxes show location of Figure 5.

high northern latitudes [*Cavanaugh et al*., 2007], MLA data are available only for the northern hemisphere of Mercury. Since the MESSENGER orbit is subpolar, at lower latitudes and at the very pole, the gaps between MLA profiles are wide; therefore, only in a circumpolar zone is the density of profiles sufficient to obtain roughness maps of a resolution comparable to the Moon (with Lunar Orbiting Laser Altimeter (LOLA) data) and Mars (with Mars Orbiter Laser Altimeter (MOLA data)). The northern boundary of the high-data density zone is 84°N, and the southern boundary is less sharp; we choose 65°N. The total area of the selected zone is only 4.4% of the whole planet. Figure 1 shows an image mosaic for this zone as context.

We used only ranging data obtained with an incidence angle lower than 30° in order to exclude noisy data. For the same reason, we use only Channel 0 measurements. Channel 0 provides the highest ranging precision; it suffers, however, from lower sensitivity (see *Cavanaugh et al*. [2007] for details about MLA channels). Our analysis shows that a higher noise in Channel 1 would bias the result by a noticeable spurious increase of the derived roughness in the smoothest areas. This increase is negligible in rough terrains, where the proportion of successful Channel 0 measurements are lower; in principle, selective inclusion of Channel 1 measurements for rough terrains might make sense; however, we choose a conservative approach and restrict processing to Channel 0 data, despite the fact that in the roughest sites we lose about half of the potentially available data points.

Topographic roughness depends on spatial scale; this dependence is fundamental and of high interest. To characterize this, we map roughness for a set of three baselines l. For each MLA shot, we find shots about a half baseline ahead and a half baseline behind along the profile and calculate a proxy for the second derivative ("curvature"), c, of along-orbit topographic profiles according to the following equation:

$$c = 4\,(h_+ + h_- - 2h)/(l_+ + l_-)^2, \tag{1}$$

where h, h_+, and h_- are surface elevations at the given laser shot, and shots a half baseline ahead and a half baseline behind, respectively, and l_+ and l_- are the distances between the shots, so $l_+ + l_- \approx l$. The most common distance between consecutive shots along a single profile is about 0.35 km. One of the baselines we use is the shortest possible baseline of $l = 2 \times 0.35$ km = 0.7 km. Analogous to the lunar map [*Kreslavsky and Head*, 2012; *Kreslavsky et al*., 2013], we also use two baselines longer by factors of 4 and 16, that is, l = 2.8 km and l = 11 km. For the shortest baseline, we always use three consecutive shots along the orbit. Due to the high eccentricity, the shot-to-shot distance along MLA profiles is not as constant as for LOLA and MOLA data; therefore, for longer baselines the chosen shots are not necessarily the fourth and sixteenth shots along the profile, as was the case in the analysis of the LOLA data. We selected only those triplets of shots where $0.35\,l \le l_+, l_- \le 0.7\,l$, where l is the "nominal" baseline of 0.7, 2.8, and 11 km; this provided proximity of the total length of the triplet $l_+ + l_-$ to the nominal baseline l. For highly asymmetric triplets, where l_+ and l_- differ significantly from each other, equation (1) is not a good approximation for the second derivative; we excluded such triplets imposing constraint $0.9 \le l_+/l_- \le 1.1$. As a result of all analysis, including the limitations described, we obtained about 4×10^6 good curvature points c for the shortest baseline and about 7×10^6 for each longer baseline.

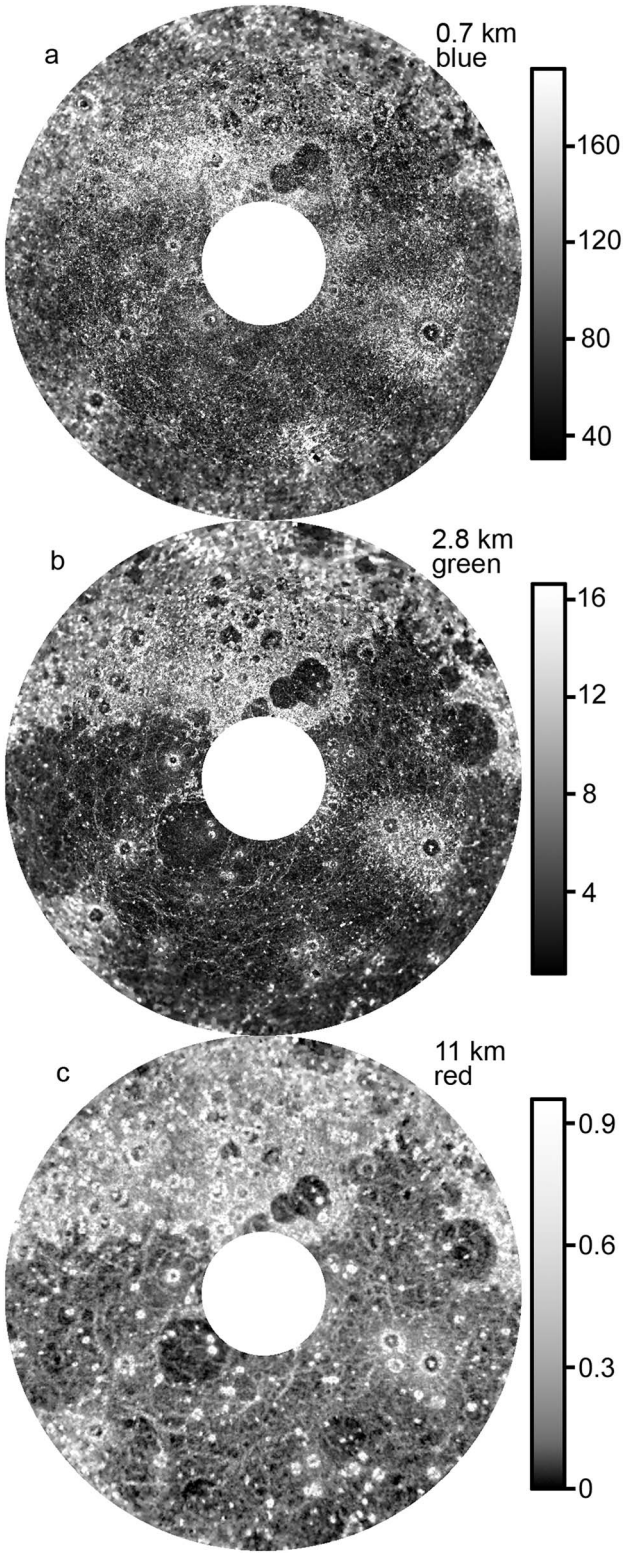

Figure 2. Topographic roughness maps of the northern circumpolar region of Mercury (Figure 1) at three baselines: (a) 0.7 km, (b) 2.8 km, and (c) 11 km. Brighter shades denote rougher surface. Absolute values of roughness are in units of 10^{-6} m^{-1} or m/km^2. The long baseline map (Figure 2c) is nonlinearly stretched to emphasize roughness variations in smoother areas. The projection is the same as in Figure 1.

We build the map in Lambert azimuthal equal area projection at a resolution of 16 pixels per degree, which is about 2.7 km per pixel. For each map pixel, we find all calculated c values located within the distance R_{pix} from the center of the pixel. For baselines l = 0.7 km and l = 2.8 km, we use the shortest possible R_{pix} = 1.9 km (half diagonal of a pixel) within 84°N–70°N latitude zone and R_{pix} = 3.8 km for 70°N–65°N, where data density is lower; for the longest baseline, l = 11 km, we use R_{pix} = 3.8 km everywhere. We consider pixels having too few points (less than 20) as having no data.

For each pixel, we considered the frequency distribution of the curvature c and calculated the quartiles $c_{1/4}$, $c_{3/4}$ of this distribution. We use the inter quartile range of this distribution, $r = c_{3/4} - c_{1/4}$, as a measure of the distribution width and thus a measure of roughness. A description of the rationale for our choice of this measure of roughness is found in *Kreslavsky et al.* [2013]. Pixels with no data (about 15% of all pixels, mostly at lower latitudes in the zone chosen) were filled with interpolated values with a heuristic algorithm striving to preserve visual sharpness.

The measure of roughness used by *Yang et al.* [2013], the median absolute value of differential slope, is not identical but is rather similar to the interquartile range of curvature used here. Experience in mapping of roughness on Mars with both measures [*Kreslavsky and Head*, 2000, 2002] indicates that the maps are hardly distinguishable visually. The roughness measure we use here is slightly more tolerant to missing data points and thus gives better statistics and, hence, lower noise. There are also some differences in details of the processing algorithms, which provide a lower noise and higher visual sharpness of our map.

Figure 2 presents three roughness maps at the three baselines in gray scale representation; lighter shades mean rougher surfaces. Figure 3 shows a color composite of roughness maps at 11 km,

Figure 3. Topographic roughness map of the northern circumpolar region of Mercury (Figure 1). Blue, green, and red channels of this color composite represent roughness maps at the three baselines of 0.7 km, 2.8 km, and 11 km, respectively, with a different nonlinear stretch that optimizes visual perception of the map. Brighter shades denote rougher surface.

2.8 km km, and 0.7 km for the red, green, and blue channels, respectively; the stretch in each channel was chosen individually to optimize the visual perception of the maps. A greater intensity in each channel denotes higher roughness, which means that generally brighter shades correspond to generally rougher surfaces. Color variations characterize the scale dependence of roughness. Reddish to yellowish shades mean the relative prevalence of larger-scale roughness, while bluish shades mean the prev alence of smaller-scale roughness.

3. Inferences About Regolith Processes

The most obvious feature of the kilometer-scale roughness map (Figures 2 and 3) is the dichotomy between the smooth northern plains [*Head et al*., 2011], which are indeed smooth (dark in roughness maps), and the surrounding cratered terrains that are rough (bright), analogous to the dichotomy between smooth maria and rough highlands on the Moon [*Rosenburg et al*., 2011; *Kreslavsky et al*., 2013]. On the Moon, the sharp roughness contrast across the geologic contacts becomes less expressive and often disappears for the shortest, hectometer baseline. This has been explained [*Kreslavsky et al*., 2013] as a result of regolith formation and reworking of the surface with subbaseline-sized craters. In other words, at the hectometer baseline, surface topography is controlled by equilibration of roughening due to formation of a saturated hectometer-scale crater population and smoothing due to regolith gardening processes. Figure 4 shows how the difference between the median roughness calculated over lunar maria and highlands diminishes at the shortest baselines.

We calculated the median values of roughness (Figures 2a and b) over large (>30% of the mapped area) typical areas of smooth plains and rough terrains on Mercury. Although the outline of the typical areas used is somewhat subjective, we found that the median roughness is not sensitive to the particular choice of the areas. Figure 4 shows that similarly to the Moon, the roughness contrast between smooth plains and rough terrains is weaker at shorter baselines; however, this contrast decrease occurs at longer baselines than on the Moon. Figure 4 suggests that on Mercury the equilibrium with regolith gardening is reached at scales a factor of 3 longer. This in turn suggests more intensive regolith gardening and/or a thicker regolith on Mercury.

What causes more intensive regolith formation and/or reworking on Mercury in comparison to the Moon? The micrometeoritic bombardment on Mercury has been argued to be much more intensive than on the Moon in terms of both mass flux and impact velocity [*Cintala*, 1992; *Borin et al*., 2009], which causes much more intensive regolith gardening on Mercury. *Neukum et al*. [2001] obtained a Mercury/Moon cratering ratio of about 1.1–1.2 for decameter to kilometer size craters. Given the uncertainties of the ratio estimation method, this means essentially the same rate of formation of primary craters. A higher escape velocity and gravity increase the relative rate of formation of secondary craters per each primary, which in turn increases regolith formation rate in comparison to the Moon. A significantly higher solar UV flux on Mercury favors dust levitation; if dust levitation significantly contributes to regolith transport [*Garrick-Bethell et al*., 2011], the higher UV flux would also increase the regolith mobility. If diurnal thermal expansion makes a significant contribution to regolith formation through disintegration of rocks [e.g., *Molaro and Byrne*, 2012], then the

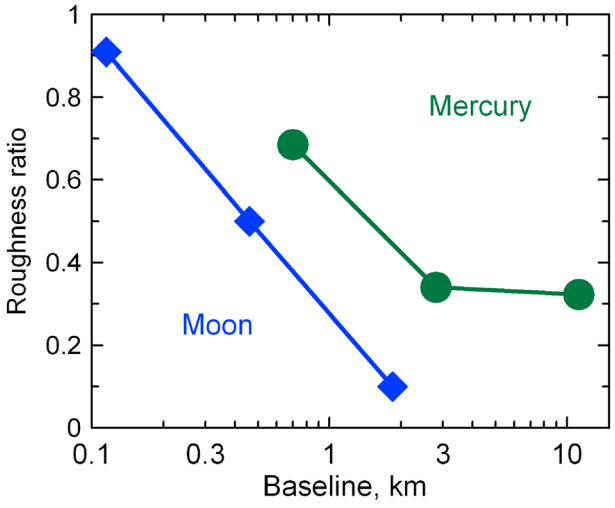

Figure 4. Ratio of the median roughness of smooth plains and cratered terrains on Mercury and mare and highlands on the Moon plotted against baseline. Low ratio means high contrast between rough and smooth terrains. Mercury trend is shifted from the Moon trend toward longer baselines by a factor of 3.

higher day/night temperature amplitude on Mercury speeds up regolith formation, while a longer solar day on Mercury works in the opposite direction.

4. Inferences About Smooth Plains

Although variations of roughness within the northern plains are much smaller than the roughness contrast between the plains and the cratered terrains, they still are well above the noise level. They are especially well seen at the longest baseline (11 km, Figure 2c). The northern rise (a broad topographic rise within the northern plains) does not display any noticeable roughness signature, which is consistent with the rise being unrelated to surface material em placement and being caused by tectonic uplift [*Zuber et al.*, 2012].

The smoothest areas in the mapped latitude zone are (presumably volcanic) plains filling large craters Henri (diameter D = 160 km) and Lismer (D = 140 km) (H and L in Figure 1), a central part of Mendelssohn basin (M in Figure 1), the whole Goethe basin (D = 300 km) and one more circular (D = 200 km) unnamed feature amid northern smooth plains centered at 74°N, 28°E shown with a circle in Figure 1 and referred as "The Circle" hereafter.

The latter two features are of special interest: their boundaries are perfectly circular and the roughness contrast across the boundary is very sharp. These features have been considered by *Klimczak et al.* [2012, Figures 2 and 3] as type examples of Type 2 ghost craters on Mercury. Type 2 ghost craters have a distinctive tectonic pattern: they are outlined by circular wrinkle ridges and have graben in their interiors. This assemblage of tectonic features has been explained by *Klimczak et al.* [2012] as a combination of global wrinkle-ridge-forming compression and local extension caused by cooling of thick lavas filling the preexisting craters or basins.

Roughness maps of the Moon and Mars contain many examples of known geological boundaries between different volcanic plain units associated with sharp roughness contrasts; commonly, smoother volcanic plains on the Moon and Mars are younger than rougher plains [*Kreslavsky et al.*, 2013]. Both on the Moon and Mars, the increased roughness of older plains is partly due to wrinkle ridges. Goethe and The Circle have fewer wrinkle ridges than the surroundings, and those ridges are gentler; however, comparison of the roughness maps (Figure 2c) and images (Figure 1) shows that the difference in ridges does not account for the roughness contrast. Here the roughness maps have the advantage of capturing typical background topo graphic variations obscured in the images by more pronounced individual features. The sharp roughness contrast associated with Goethe and The Circle suggests that these features are not purely tectonic but are distinctive material units. It is probable that they are volcanic plain-forming flows postdating the flows that formed the northern plains [*Head et al.*, 2011]. Color Mercury Dual Imaging System (MDIS) mosaics do not show any sharp spectral contrasts associated with the boundaries of these units [*Head et al.*, 2011; *Denevi et al.*, 2013]; however, the quality of color data at these high latitudes is inherently low (because they are always imaged under low Sun).

The ridges that outline Goethe and The Circle are very similar and somewhat different in their morphology in comparison to typical wrinkle ridges on Mercury. The outlining circular ridges have a rather sharp outward facing scarp, which is not typical of wrinkle ridges (Figure 5). They also have a shorter scale of sinuosity (Figure 5). The position of the roughness contrast coincides with the position of the outlining ridges within the map resolution; the resolution does not allow an assessment of whether the roughness boundary follows

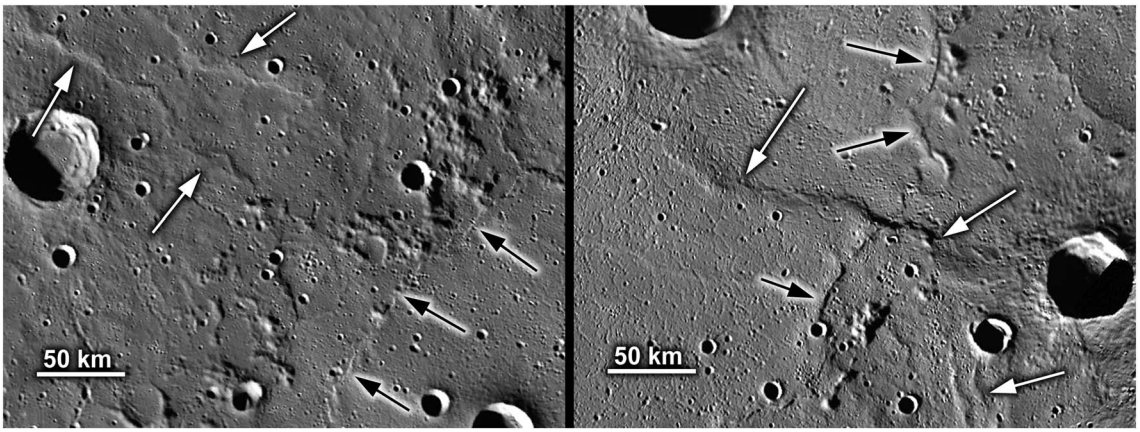

Figure 5. Scarp encircling Goethe basin (black arrows) in comparison to typical wrinkle ridges (white arrows). Portions of MDIS global mosaic; the same projection as in Figure 1.

the small-scale sinuosity of the ridges. It is possible that the outward scarps are actually fronts of thick flows forming the smooth volcanic units of Goethe and The Circle.

Thus, we would suggest the following sequence events in this part of Mercury: (1) impacts form Goethe and The Circle basins, (2) northern plains are formed by flood volcanism, and lavas fill or partly fill the basins, (3) lava-loaded basins subside, and two craters form inside Goethe, (4) new flood lavas fill Goethe and The Circle, (5) graben form in these new lavas by the mechanism discussed by *Klimczak et al*. [2012], and (6) the northern rise forms by deformation. The formation of wrinkle ridges may be transgressive through steps 3–6.

There are some other somewhat smoother areas in Figure 2c, also associated with ghost craters; however, the roughness contrast does not appear as sharp as in the cases of Goethe and The Circle, which may or may not be due to lack of data. There is a possibility that in these cases, we are also dealing with analogous distinctive material units, but it is not as clear as for Goethe and The Circle.

5. Conclusions

We present a map of the multiscale topographic roughness of the northern circumpolar area of Mercury. The map captures the regional variations of the typical background topographic texture of the surface. Unlike in the cases of LOLA data for the Moon and MOLA data for Mars, the MLA data allow high-quality roughness mapping only for a small part of the surface of the planet. The map shows the clear dichotomy between smooth northern plains and rougher cratered terrains. The lowered contrast of this dichotomy at the shortest (0.7 km) baseline indicates that regolith on Mercury is thicker, and/or gardening processes are more intensive in comparison to the Moon, approximately by a factor of 3. The map reveals sharp roughness contrasts within northern plains of Mercury that we interpret as geologic boundaries of volcanic plains of different age.

Potentially, the analysis of the roughness map can be useful for other studies. For example, the mapped area contains a young 100 km size crater Stieglitz with an impressive roughness signature; it would be interesting to compare it with analogous craters on the Moon. Roughness of cratered terrains in the mapped area is lower than that of lunar highlands. Analysis of this difference is another interesting study that can be done with the map.

Acknowledgments
Source data used in this study are freely accessible through NASA Planetary Data System. New roughness maps are available online at http://planetary.brown.edu. M.A.K. greatly acknowledges being hosted by MIIGAiK and supported by Russian Science Foundation project 14-22-00197. We gratefully acknowledge financial support for this analysis from the MESSENGER mission (DTM 3250–05) and the Lunar Reconnaissance Orbiter (LRO) Lunar Orbiting Laser Altimeter (LOLA) (NASA grants NNX11AK29G and NNX13A077G) to J.W.H.

The Editor thanks two anonymous reviewers for their assistance in evaluating this paper.

References

Borin, P., G. Cremonese, F. Marzari, M. Bruno, and S. Marchi (2009), Statistical analysis of micrometeoroids flux on Mercury, *Astron. Astrophys.*, *503*, 259–264, doi:10.1051/0004-6361/200912080.

Cavanaugh, J. F., et al. (2007), The Mercury laser altimeter instrument for the MESSENGER mission, *Space Sci. Rev.*, *131*, 451–479, doi:10.1007/s11214-007-9273-4.

Cintala, M. J. (1992), Impact-induced thermal effects in the lunar and Mercurian regoliths, *J. Geophys. Res.*, *97*, 947–973, doi:10.1029/91JE02207.

Denevi, B. W., et al. (2013), The distribution and origin of smooth plains on Mercury, *J. Geophys. Res. Planets*, *118*, 891–907, doi:10.1002/jgre.20075.

Garrick-Bethell, I., J. W. Head, and C. M. Pieters (2011), Spectral properties, magnetic fields, and dust transport at lunar swirls, *Icarus*, *212*, 480–492, doi:10.1016/j.icarus.2010.11.036.

Head, J. W., et al. (2011), Flood volcanism in the Northern high latitudes of Mercury revealed by MESSENGER, *Science*, *333*, 1853, doi:10.1126/science.1211997.

Klimczak, C., T. R. Watters, C. M. Ernst, A. M. Freed, P. K. Byrne, S. C. Solomon, D. M. Blair, and J. W. Head (2012), Deformation associated with ghost craters and basins in volcanic smooth plains on Mercury: Strain analysis and implications for plains evolution, *J. Geophys. Res.*, *117*, E00L03, doi:10.1029/2012JE004100.

Kreslavsky, M. A., and J. W. Head (2000), Kilometer-scale roughness of Mars: Results from MOLA data analysis, *J. Geophys. Res.*, *105*, 26,695–26,712, doi:10.1029/2000JE001259.

Kreslavsky, M. A., and J. W. Head (2002), Mars: Nature and evolution of young latitude-dependent water-ice-rich mantle, *Geophys. Res. Lett.*, *29*, 1719, doi:10.1029/2002GL015392.

Kreslavsky, M. A., and J. W. Head (2012), New observational evidence of global seismic effects of basin-forming impacts on the Moon from Lunar Reconnaissance Orbiter Lunar Orbiter Laser Altimeter data, *J. Geophys. Res.*, *117*, E00H24, doi:10.1029/2011JE003975.

Kreslavsky, M. A., J. W. Head, G. A. Neumann, M. A. Rosenburg, O. Aharonson, D. E. Smith, and M. T. Zuber (2013), Lunar topographic roughness maps from Lunar Orbiter Laser Altimeter (LOLA) data: Scale dependence and correlation with geologic features and units, *Icarus*, *226*, 52–66, doi:10.1016/j.icarus.2013.04.027.

Molaro, J., and S. Byrne (2012), Rates of temperature change of airless landscapes and implications for thermal stress weathering, *J. Geophys. Res.*, *117*, E10011, doi:10.1029/2012JE004138.

Neukum, G., J. Oberst, H. Hoffmann, R. Wagner, and B. A. Ivanov (2001), Geologic evolution and cratering history of Mercury, *Planet. Space Sci.*, *49*, 1507–1521, doi:10.1016/S0032-0633(01)00089-7.

Rosenburg, M. A., O. Aharonson, J. W. Head, M. A. Kreslavsky, E. Mazarico, G. A. Neumann, D. E. Smith, M. H. Torrence, and M. T. Zuber (2011), Global surface slopes and roughness of the Moon from the Lunar Orbiter Laser Altimeter, *J. Geophys. Res.*, *116*, E02001, doi:10.1029/2010JE003716.

Yang, D., M. T. Zuber, G. A. Neumann, D. E. Smith, J. W. Head, and S. C. Solomon (2013), Distribution of topographic slope and roughness in Mercury's northern hemisphere, Lunar and Planetary Sci. Conf. XLIV, Abstract 2347, The Woodland, Tex.

Zuber, M. T., et al. (2012), Topography of the northern hemisphere of Mercury from MESSENGER laser altimetry, *Science*, *336*, 217, doi:10.1126/science.1218805.